Strongly constrained and appropriately normed density functional theory exchange-correlation functional applied to rare earth oxides

Alvaro Adrian Carrasco Alvarez,[1,2,*] Manuel Bibes,[2] Wilfrid Prellier,[1] and Julien Varignon[1]
[1]*Laboratoire CRISMAT, CNRS UMR 6508, ENSICAEN, Normandie Université, 6 boulevard Maréchal Juin, F-14050 Caen Cedex 4, France*
[2]*Unité Mixte de Physique, CNRS, Thales, Université Paris Sud, Université Paris-Saclay, F-91767 Palaiseau, France*

(Received 26 October 2022; revised 2 February 2023; accepted 10 February 2023; published 6 March 2023)

Density functional theory (DFT) is one of the main tools for studying the electronic structure of solids and molecules. Nevertheless, one of the main drawbacks of the implementation of DFT is the so-called self-interaction error (SIE) that can yield undesired delocalization errors and ultimately results in the prediction of metals instead of experimentally observed insulators. These SIEs can be amended by using more evolved exchange-correlation functionals than standard local density approximation such as the recent meta-generalized gradient approximation strongly constrained and appropriately normalized (SCAN) functional that is successful in describing electronic properties of $3d$ transition metal oxides. Nevertheless, the ability of such a functional to describe electronic properties of materials involving more localized states such as $4f$ orbitals is rather elusive. Here, we show that, even though SCAN can sometimes predict the insulating character of some compounds, it often fails in predicting the correct band edge orbital character of insulators. By comparing our SCAN results with benchmark simulations obtained with more accurate hybrid DFT calculations, we ascribe this failure to insufficiently amended SIEs by SCAN that results in an underestimation of Hund's splitting associated with $4f$ states. Thus, although appropriate for $3d$ transition metal elements, the SCAN functional is not yet a sufficient platform for studying electronic properties of materials involving rare-earth elements where $4f$ states play a key role in the properties.

DOI: 10.1103/PhysRevB.107.115109

I. INTRODUCTION

Density functional theory (DFT) is a workhorse technique in material science allowing us to study the electronic properties of solids and molecules. It reformulates the many-body problem in terms of the sole electron density $\rho(\vec{r})$, allowing us to compute any ground state observable as a function of $\rho(\vec{r})$ [1,2]. Its practical implementation nevertheless relies on the introduction of a fictitious auxiliary problem with noninteracting particles but that yields the very same ground state density [3], allowing us to obtain the energy of the system as a functional of the electron density [1–3]. This functional must implement the exchange and correlation (xc) phenomena, but the exact functional is unknown. Thus, the practical implementation of DFT relies on the accuracy of the functional that is used to model the energy in terms of the electronic density. The most challenging part of the practical DFT is to construct the effective potential that properly reproduces the electron-electron interactions (the xc functional) and is in fact the main source of error in DFT—the xc functional also must contain the kinetic energy difference between the real system and the fictitious noninteracting system. Among the different inaccuracies that are present in DFT, there is one type of error called a self-interaction error (SIE) originating from the fact that the effective potential that is used for each of the electrons considers some of the potential that is created by the same electron. This effect can thus yield undesired delocalization errors that can be dramatic for correlated systems involving localized orbitals (e.g., $3d$ or $4f$ orbitals).

There are different approximations of the xc functional that are usually classified on a Jacob's ladder [4]. The first rung corresponds to the local density approximation (LDA) [5,6], where the xc depends only on the density. The second rung adds a dependency with the derivative of the density [generalized gradient approximation (GGA)] [7], while the third one entails meta-GGA functionals [8] such as the strongly constrained and appropriately normalized (SCAN) functional [9] that add a dependance of the xc functional on the Kohn-Sham orbitals kinetic energy. All these rungs correspond to local or semilocal xc functionals of the noninteracting density matrix and do not make a distinction between occupied and unoccupied states. Fourth-rung DFT xc functionals correspond to nonlocal functionals of the occupied orbitals and hence make a distinction between occupied and unoccupied states. These functionals entail (i) DFT + U methods [10,11], where an empirical Hubbard-like potential U acts on a subset of orbitals—i.e., the correlated states—and adds an energy penalty for delocalizing an electron and (ii) hybrid DFT functionals in which SIEs are reduced by adding a fraction of the exact Hartree-Fock exchange to a combination of LDA, GGA, or meta-GGA functionals [12–16].

Unlike DFT + U methods where the U parameter is empirical and case dependent, parameter-free DFT xc functionals are extremely attractive since they can adapt to different formal oxidation states (FOSs) that a cation can show in a compound.

*alvaro-adrian.carrasco-alvarez@ensicaen.fr

This is the case, for instance, in oxides showing a metal-insulator transition associated with the formation of a double local environment for cations (e.g., $SrBiO_3$ with Bi^{3+}/Bi^{5+} cations or $RNiO_3$ with Ni^{2+}/Ni^{4+} cations in their insulating phase) [17–21] or in doped compounds formed at interfaces or by making solid solutions with other elements. To that end, it is important to assess the ability of a functional to model electronic properties of model systems, with a reasonable computational cost. Recently, the meta-GGA SCAN functional has been shown to be able to predict the correct metallic or insulating character of correlated $3d$ transition metal oxide perovskites [22], cuprates [23,24], binary oxides [25], or doping effects in rare-earth nickelates and bismuth oxide superconductors [26,27]. However, this functional somehow overestimates the magnetic moment of the ions and might predict the wrong magnetic ground state [28–32]. This is mainly due to the tendency of the SCAN functional to produce more localized states than usual GGA functionals, which in the case of open shell metallic compounds might not be completely appropriate [33,34]. Furthermore, it seems that the performance of the functional is not completely uniform, depending on the system when calculating the hyperfine coupling constants of transition metals [30].

Although the SCAN functional overall captures the proper electronic properties of oxides with a $3d$ transition metal element [22], its ability to model properties of compounds with more localized electronic states such as $4f$ elements is elusive. Here, we compare the reliability of SCAN on $4f$ elements-based oxide perovskites by comparing the electronic structure with more sophisticated hybrid DFT calculations. We find that SCAN fails to predict the insulating behavior in some compounds, and even though a gap is predicted, the band edge orbital characters (BEOCs) are wrongly assigned. This is ascribed to an erroneous localization of $4f$ states too close to the Fermi level with SCAN, suggesting that Hund's rule and crystal field splitting are not well considered by SCAN for $4f$ elements. Thus, SIEs of oxides with partially filled $4f$ states are likely not properly amended by the SCAN functional, and consequently, any analysis of the physics of these compounds should carefully consider these limitations.

II. METHODS

A. Strategy

To understand the successes and limitations of the SCAN functional for modeling the electronic structure of correlated oxides with $4f$ elements, we devise a three-step strategy. Firstly, we relax the structure of the different compounds using the SCAN [9] functional and keeping the $4f$ electrons as an effective core. Secondly, we follow the same procedure but treating the $4f$ states as valence electrons, still using the SCAN functional. Finally, we use the relaxed structure of step 2 as an input for a single self-consistent calculation with the hybrid functional HSE06 [14], and we compare it with the electronic structure obtained at step 2. This choice is guided by the fact that (i) hybrid functionals usually provide a correct band gap description [35] and (ii) HSE06 has been tested on several rare-earth oxides [36–38] and rare-earth pnictides [39], giving $<15\%$ of error on the band gap amplitude with respect to experiment and predicting lattice parameters and BEOCs matching experiments.

B. Choice of compounds

We perform our study on selected compounds encompassing $Eu^{2+}\,TiO_3$, $Gd^{3+}\,TiO_3$, $Pr^{3+}\,CrO_3$, and $Dy^{3+}\,FeO_3$. The first two compounds are isoelectronic with a $4f^7$ electronic configuration but with different FOS of A-site cations. The other two compounds deviate from the half-filling situation with Pr^{3+} holding two electrons and Dy^{3+} possessing nine electrons. Thus, we may access the role of $4f$ fillings and FOSs on the SIE in rare-earth elements-based oxide perovskites.

C. Other details

Core electrons are treated using the projector augmented-wave (PAW) method [40] with the following PBE PAW datasets: Eu, Eu_3, Ti, O, Gd, Gd_3, Pr, Pr_3 Cr, Dy, Dy_3, Fe, Ni, and La—the notation _3 refers to the PAW treating $4f$ electrons as core electrons. The structural relaxations (cell parameters plus atomic positions) are performed until the forces acting on each atom are $<1\,\mathrm{meV/Å}$. Spins are only treated at the colinear level. Magnetic and structural structures are limited to the observed symmetries at low temperature (see Table I). The energy cutoff is set to 650 eV, and we use an $8\times8\times6$ Γ-centered k-mesh for the 4-f.u. cell corresponding to a $(\sqrt{2},\sqrt{2},2)$ supercell with respect to the primitive high-symmetry *Pm*-3*m* cubic cell adopted by ABO_3 perovskite oxides. In the case of the HSE06 functional, we reduced the k-mesh to a $6\times6\times4$ Γ-centered k-mesh for the single self-consistent calculation for computational cost reasons. We perform *ab initio* calculations with DFT using the Vienna *Ab initio* Simulation Package [56–58], version 6.2.1. We used the standard parametrization of HSE06 functional with 25% of exact exchange and a range separation parameter $\mu = 0.2\,\mathrm{Å}^{-1}$. Unfolded band structures are obtained using VaspBandUnfold software [59,60].

III. RESULTS AND DISCUSSION

A. Structural relaxation with $4f$ electrons and SCAN functional

We summarize in Table I the optimized lattice parameters obtained after the structural relaxation with the SCAN functional with treating $4f$ electrons as well as all relevant quantities such as the band gap amplitude, BEOCs extracted from a projected density of state (pDOS) analysis, and computed rare-earth magnetic moments obtained with the three different procedures. For the four tested compounds, the structural relaxation performed with the SCAN functional is in good agreement with reported lattice parameters from experiments at low temperature, yielding $<1\%$ of error on the total volume. Regarding magnetic moments, we get quantities either with SCAN or HSE06 that are compatible with the formal electron count for each element but also with experiments when values are available. We discuss in the following sections the case-to-case electronic structure in more detail.

TABLE I. Summary of quantities extracted from first-principles calculations on selected perovskite oxides with $4f$ elements. Structural relaxation results are reported for the SCAN + $4f$ electrons included.

Compound	$4f$ conf.	Mag order	Space group	Procedure	a(Å)	b (Å)	c (Å)	Band gap (eV)	BEOC	μ_R (μ_B)
$EuTiO_3$	$4f^7$	Eu: G-AFM [41]	I_4/mcm [42]	SCAN, no $4f$				2.10	(O p, Ti d)	–
				SCAN, with $4f$	5.47	5.47	7.89	0.00	–	6.68
				HSE06, with $4f$				0.73	(Eu f, Ti d)	6.79
				exp.	5.52	5.52	7.82 [42]	0.93 [43]	(Eu f, Ti d)	6.93 [41]
$GdTiO_3$	$4f^7$	Gd: FM, Ti: FM, AFM order between A and B [44,45]	*Pbnm* [44]	SCAN, no $4f$				0.06	(Ti d, Ti d)	–
				SCAN, with $4f$	5.36	5.72	7.65	0.06	(Ti d, Ti d)	6.90
				HSE06, with $4f$				1.60	(Ti d, Ti d)	6.90
				exp.	5.40	5.70	7.68 [44]	0.70–1.80 [46,47]	(Ti d, Ti d)	–
$PrCrO_3$	$4f^2$	Pr: C-AFM, Cr: G-AFM [48–50]	*Pbnm* [48]	SCAN, no $4f$				2.19	(Cr d, Cr d)	–
				SCAN, with $4f$	5.42	5.48	7.71	0.74	(Pr f, Pr f)	1.96
				HSE06, with $4f$				3.34	(Pr f, Cr d)	1.96
				exp.	5.44	5.47	7.71 [48]	3.2–3.26 [48,51]	(Pr f, Cr d)	–
$DyFeO_3$	$4f^9$	Dy: G-AFM, Fe: G-AFM [52,53]	*Pbnm* [52]	SCAN, no $4f$				1.27	(O p, Fe d)	–
				SCAN, with $4f$	5.27	5.58	7.59	1.12	(O p, Fe d)	4.92
				HSE06, with $4f$				2.91	(O p, Fe d)	4.94
				exp.	5.30	5.59	7.61 [52]	2.10–2.60 [54,55]	(O p, Fe d)	–

B. SCAN fails to predict electronic properties in the simple perovskite system $EuTiO_3$

We first consider $EuTiO_3$ that is isostructural to $SrTiO_3$ by showing a tetragonal I_4/mcm cell at low temperature [42] characterized by a $a^0\,a^0\,c^-$ octahedral rotation pattern using Glazer's notation [61]. Unlike $SrTiO_3$ that is a band insulator with a gap approaching 4 eV between filled O p states and empty Ti d states, Eu^{2+} cations present a half-filled $4f^7$ configuration, and hence, $EuTiO_3$ is a Mott insulator with a gap of 0.93 eV formed between Eu $4f$ states and empty Ti $3d$ states [43]. If one neglects the $4f$ electrons of Eu ions, we recover a band insulating compound very similar to $SrTiO_3$ [see Table I and Fig. 1(a)]. However, this is incompatible with experimental facts. When $4f$ electrons are explicitly included in the simulation, the electronic structure of the compound is sensibly altered, as inferred by the pDOS reported in Fig. 1(b). The gap between O p and Ti d states remains similar, but Eu $4f$ states are now localized inside this gap. Nevertheless, these states sit just at the bottom of the conduction band formed by Ti d states, and the Fermi level crosses the Eu states. It ultimately yields a metallic character, at odds with the experimentally observed insulating regime. This is also in sharp contrast with the one-shot HSE06 calculation that mostly reproduces the same electronic structure as SCAN with $4f$ electrons but in which a gap of 0.73 eV is formed between occupied Eu $4f$ states and unoccupied Ti d states. By carefully inspecting the pDOS of Figs. 1(b) and 1(c), one can appreciate a weaker hybridization between Eu f and O p/Ti d states at the bottom of the conduction band, suggesting that HSE06 better localizes the $4f$ states than the SCAN functional, i.e., delocalization errors are still too large for the SCAN functional. Hund's rule acting on the $4f$ states is evaluated to 5.4 and 8.4 eV with SCAN and HSE06 functionals, respectively. Thus, the occupied $4f$ states will be sufficiently pushed down in between the O $p-$ Ti d states, therefore producing a gap with HSE06, while SCAN will locate these states at the bottom of the conduction band. Even with an *a priori* simple compound without any orbital degeneracies, the SCAN functional cannot yet reproduce the insulating character of $EuTiO_3$ due to an underestimated Hund's splitting on $4f$ states.

C. Influence of the FOS

To better understand the failure of SCAN in capturing the insulating character of material with only a half-filled configuration, we now inspect $GdTiO_3$ that is isoelectronic to $EuTiO_3$ but in which Gd is in a 3+ FOS. $GdTiO_3$ is a Mott insulator with a gap formed between occupied and unoccupied Ti d states, estimated between 0.70 to 1.8 eV in the $RTiO_3$ family (R = Lu-La, Y) [46,47]. This compound adopts an orthorhombic *Pbnm* cell characterized by the usual $a^-\,a^-\,c^+$ octahedral rotation pattern [44]. Using the SCAN functional, either with or without $4f$ electrons treated in the simulation, we correctly obtain an insulator with a narrow band gap of 0.06 eV, in agreement with previous simulations in $YTiO_3$ with SCAN [22]—this is due to the usual underestimation of band gaps with semilocal DFT xc functionals (see Table I). In this case, we can see from the pDOS of Figs. 2(a) and 2(b) that the occupied (unoccupied) Gd $4f$ states are localized

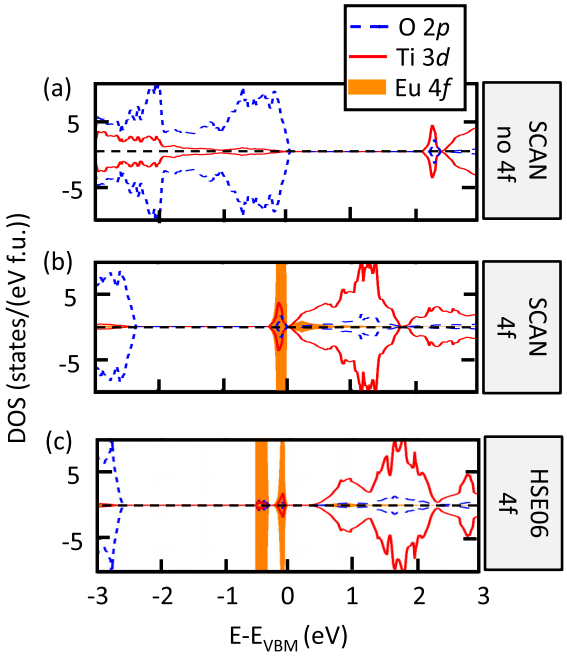

FIG. 1. Projected density of states on Ti d (red line), O p (dashed blue line), and Eu $4f$ (orange area) in $EuTiO_3$ using the meta-generalized gradient approximation (GGA) strongly constrained and appropriately normalized (SCAN) and HSE06 functionals and involving or not the $4f$ states in the simulations.

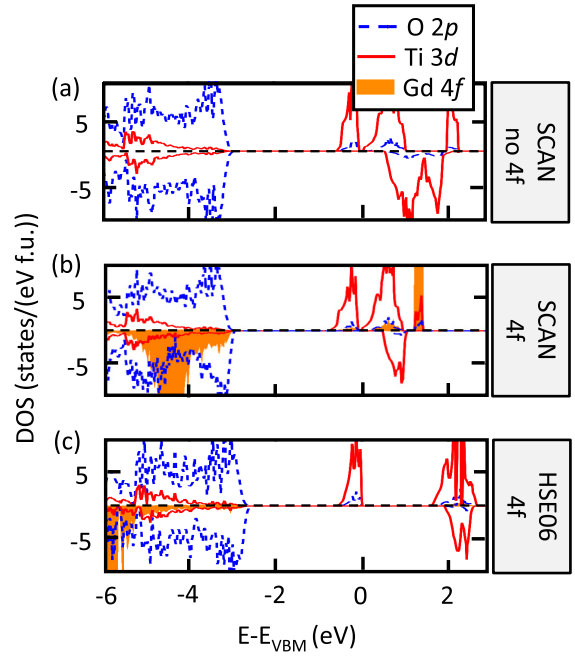

FIG. 2. Projected density of states on Ti d (red line), O p (dashed blue line), and Gd $4f$ (orange area) in $GdTiO_3$ using the meta-generalized gradient approximation (GGA) strongly constrained and appropriately normalized (SCAN) and HSE06 functionals and involving or not the $4f$ states in the simulations.

well below (above) the Fermi level, hence having no role on the BEOCs that are correctly predicted here. The success of SCAN here can be understood in terms of delocalization errors that are weaker in $Gd^{3+}TiO_3$ with respect to Eu^{2+} TiO_3: a 3+ cation will interact more with O^{2-} $2p$ states and hence will ultimately yield a more delocalized electronic structure than a 2+ cation interacting with O^{2-} anions. This is confirmed by the pDOS of Fig. 2(b) that shows a more hybridized Gd^{3+} $4f-$O $2p$ electronic structure, while Eu^{2+} $4f$ states are well separated from occupied O $2p$ states [Fig. 1(c)]. By performing the one-shot HSE06 calculation, we improve the band gap amplitude of $GdTiO_3$ and recover values obtained with DFT+U [62]. Nevertheless, one can also notice an enlargement of the splitting between occupied and unoccupied $4f$ states with the HSE06 functional, suggesting a greater Hund's splitting due to better amended SIE.

D. Failure of SCAN for materials with partly occupied $4f$ shells

After establishing the successes and failures of SCAN to model electronic properties of materials with half-filled $4f$ states, we now inspect its ability for materials with partly filled $4f$ states where one can expect larger correlation effects, hence more delocalization errors from DFT. To that end, we inspect $PrCrO_3$ and $DyFeO_3$, two perovskite oxides adopting an orthorhombic *Pbnm* structure at low temperature characterized by the usual a^- a^- c^+ octahedral rotation pattern [48,52], but that shows a $4f^2$ (Pr^{3+}) and $4f^9$ (Dy^{3+}) electronic configurations for rare earths. Both compounds are insulators with a gap formed between Pr f and Cr d and between Fe d, O p, and Fe d states in $PrCrO_3$ [48,51] and $DyFeO_3$ [54,55], respectively. By looking at the pDOS of Figs. 3(a) and 3(d), neglecting the Dy $4f$ states yields the right BEOCs in $DyFeO_3$ but not in $PrCrO_3$ where a (Cr d, Cr d) BEOC is observed. Adding the $4f$ states yields the correct Pr f character at the top of the valence band in $PrCrO_3$, but the gap is now formed with Pr $4f$ states at the bottom of the conduction band, in contrast to experiments [Fig. 3(b)]. Furthermore, the band gap becomes strongly reduced with respect to the simulation, considering the $4f$ electrons as core states (i.e., included in the PAW potential). In $DyFeO_3$, the situation also gets worse, as BEOCs are totally dominated by Dy f states, a fact not observed experimentally [Fig. 3(e)]. Once a HSE06 calculation over the SCAN + $4f$ electrons calculation is performed, the correct BEOC and gap amplitude are restored for both compounds [Figs. 3(c) and 3(f)]. One may notice that band gaps are slightly overestimated with respect to the experimental values (2.5% and 11% in $PrCrO_3$ and $DyFeO_3$, respectively). Such an overestimation is not, however, only a fact for these two compounds, but it emerged as well in Ce_2O_3, although HSE06 gives a fair agreement for other R_2O_3 (R = rare earth) members [36]. It may also originate from uncertainty with the experimental measurement. We emphasize that no experimental band gap value has been identified for $DyFeO_3$ and that values for $YFeO_3$ and $LaFeO_3$—extreme compounds of the $RFeO_3$ phase diagram—have been used. Again, by looking at pDOS, one identifies that HSE06 provides a larger splitting between occupied and unoccupied $4f$ states that are pushed down and/or up in energies in the valence and/or conduction band. This is due to an insufficient crystal field splitting on $4f$ produced by SCAN ($\Delta_{CF} \approx 0.74$ and 1.12 eV in $PrCrO_3$ and

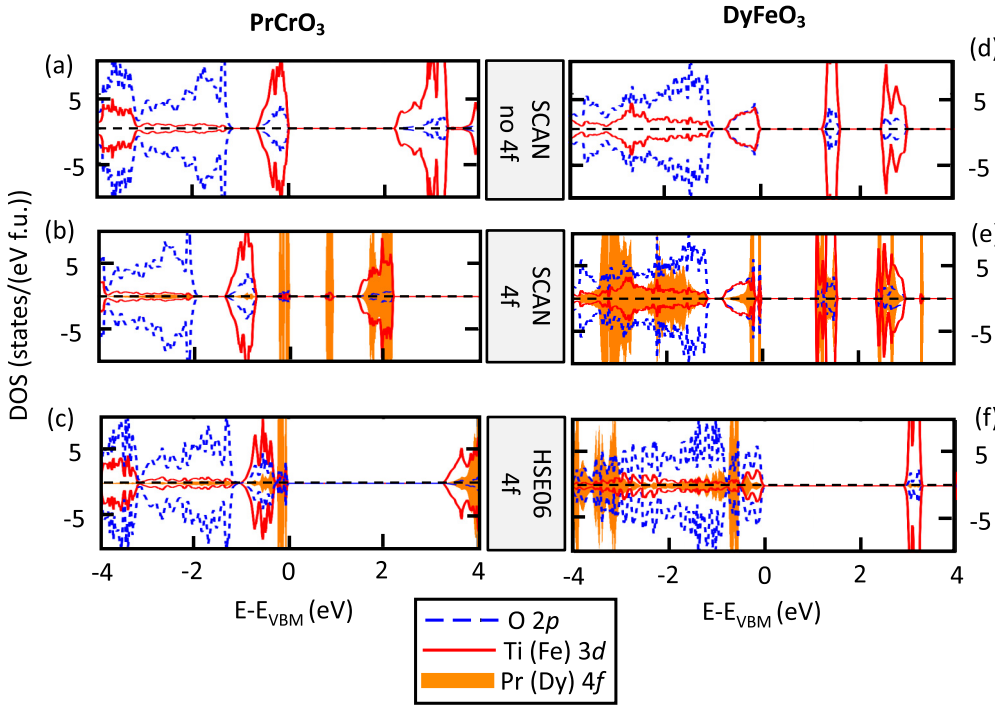

FIG. 3. Projected density of states on Ti and Fe d (red line), O p (dashed blue line), and Pr and Dy $4f$ (orange area) in $PrCrO_3$ (left panels) and $DyFeO_3$ (right panels) using the meta-generalized gradient approximation (GGA) strongly constrained and appropriately normalized (SCAN) and HSE06 functionals and involving or not the $4f$ states in the simulations.

$DyFeO_3$, respectively) with respect to HSE06 ($\Delta_{CF} \approx 3.4$ and 4.8 eV in $PrCrO_3$ and $DyFeO_3$, respectively).

E. Failure of SCAN is not limited to ABO_3 materials with a $4f$ element

We finally inspect the ability of SCAN to model properties of other compounds involving $4f$ states. This is the case of $PrNiO_2$ or $NdNiO_2$, adopting infinite layered structures based on NiO_2 planes intercalated between Pr or Nd planes along the c axis. These compounds attract a lot of interest since they become superconducting once Pr or Nd are partly substituted with a divalent cation [63–65]. Although not experimentally well known, theoretical works have suggested that both compounds adopt an undistorted tetragonal P_4/mmm cell [66–69]. By comparing our simulations of $PrNiO_2$ including $4f$ electrons using either SCAN or HSE06 with an in-plane antiferromagnetic (AFM) order, we recover a similar trend observed in ABO_3 compounds: the $4f$ states are improperly split with SCAN, thereby yielding strong Pr $4f$ state contribution at the Fermi level, while these states are pushed down and up in energies in the valence and conduction band, respectively, using the hybrid functional (Fig. 4). The failure of SCAN to correctly place the $4f$ electrons is confirmed in $LaNiO_2$ in which there are mostly no occupied $4f$ states identified in bands located around the Fermi level. The slight contribution La $4f$ states identified 0.5 eV above the Fermi level along the A-R-Z path is removed by performing the HSE06 single-shot calculation. However, this has a relatively weak impact on the bands crossing the Fermi level that remain mostly dominated by Ni d, O p, and Pr/La d states. One emphasizes that the HSE06 functional increases the bandwidth associated with the bands crossing the Fermi level, although the topology remains rather like the SCAN results. The failure of SCAN to properly place the $4f$ states is thus not limited to ABO_3 perovskites, and it may entail many other oxide compounds involving $4f$ elements.

IV. CONCLUSIONS

We have shown that the meta-GGA SCAN functional is mostly unable to properly localize and place the $4f$ bands at the right energy scale in oxide compounds. This leads to many qualitatively wrong results, as in the case of $EuTiO_3$, where SCAN cannot predict the characteristic insulating behavior of the compound. In addition, even though a gap is predicted, the BEOC is mostly predicted with wrong ion and orbital characters. These inaccuracies come from SIEs yielding delocalization errors that dramatically underestimate the Hund and crystal field splitting. Thus, the SCAN functional may be carefully employed when dealing with rare-earth elements. Therefore, there are multiple solutions to overcome the problem: (i) use another functional that has been shown to appropriately reproduce the electronic structure of these $4f$ states and benchmark the results, or (ii) employ DFT+U schemes with a Hubbard-like U parameter applied to $4f$ for amending remaining SIEs.

ACKNOWLEDGMENTS

This paper has received financial support from the CNRS through the MITI interdisciplinary programs under the project

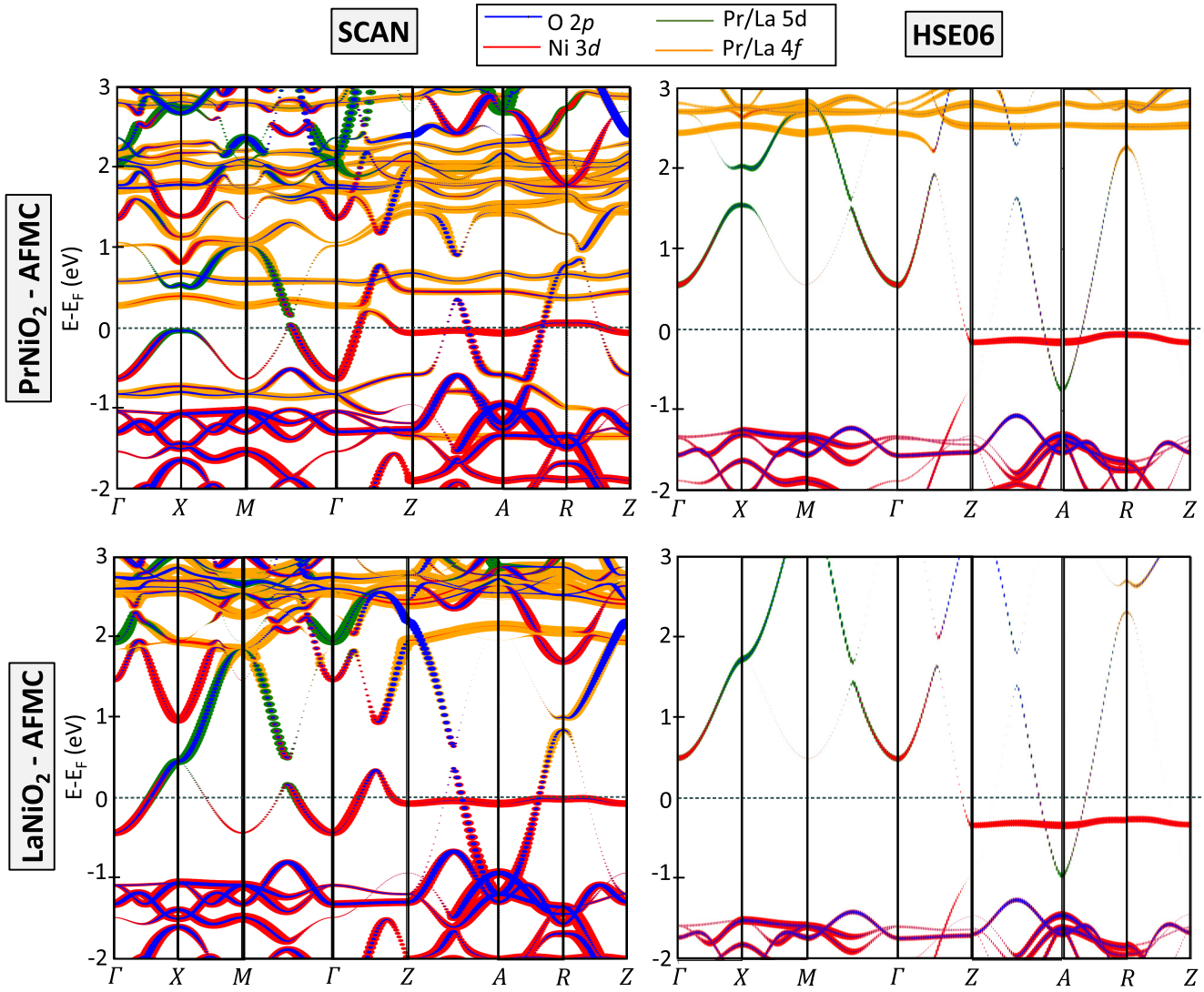

FIG. 4. Unfolded band structure to the high-symmetry primitive P_4/mmm cell of $PrNiO_2$ (top panels) and $LaNiO_2$ (lower panels) using the meta-generalized gradient approximation (GGA) strongly constrained and appropriately normalized (SCAN) (left panels) and hybrid HSE06 (right panels) functionals. Calculations are performed with C-type antiferromagnetic (AFMC) order. Coordinates of the high-symmetry points are $\Gamma(0,0,0)$, $X(\frac{1}{2},0,0)$, $M(\frac{1}{2},\frac{1}{2},0)$, $Z(0,0,\frac{1}{2})$, $A(\frac{1}{2},\frac{1}{2},\frac{1}{2})$, and $R(\frac{1}{2},0,\frac{1}{2})$.

SuNi and through the ANR SUPERNICKEL. Authors acknowledge access granted to HPC resources of Criann through Projects No. 2020005 and No. 2007013 and of Cines through the DARI Project No. A0080911453.

[1] P. Hohenberg and W. Kohn, Phys. Rev. **136**, B864 (1964).
[2] R. M. Martin, *Electronic Structure* (Cambridge University Press, Cambridge, 2004).
[3] W. Kohn and L. J. Sham, Phys. Rev. **140**, A1133 (1965).
[4] R. Car, Nat. Chem. **8**, 820 (2016).
[5] U. Von Barth and L. Hedin, J. Phys. C Solid State Phys. **5**, 1629 (1972).
[6] D. M. Ceperley and B. J. Alder, Phys. Rev. Lett. **45**, 566 (1980).
[7] J. P. Perdew, Physica B **172**, 1 (1991).
[8] J. Tao, J. P. Perdew, V. N. Staroverov, and G. E. Scuseria, Phys. Rev. Lett. **91**, 146401 (2003).
[9] J. Sun, A. Ruzsinszky, and J. P. Perdew, Phys. Rev. Lett. **115**, 036402 (2015).
[10] S. L. Dudarev, G. A. Botton, S. Y. Savrasov, C. J. Humphreys, and A. P. Sutton, Phys. Rev. B **57**, 1505 (1998).
[11] V. I. Anisimov, J. Zaanen, and O. K. Andersen, Phys. Rev. B **44**, 943 (1991).
[12] D. I. Bilc, R. Orlando, R. Shaltaf, G.-M. Rignanese, J. Íñiguez, and P. Ghosez, Phys. Rev. B. **77**, 165107 (2008).
[13] J. Heyd, G. E. Scuseria, and M. Ernzerhof, J. Chem. Phys. **118**, 8207 (2003).
[14] A. V. Krukau, O. A. Vydrov, A. F. Izmaylov, and G. E. Scuseria, J. Chem. Phys. **125**, 224106 (2006).
[15] A. D. Becke, J. Chem. Phys. **98**, 1372 (1993).
[16] C. Lee, W. Yang, and R. G. Parr, Phys. Rev. B **37**, 785 (1988).
[17] G. M. Dalpian, Q. Liu, J. Varignon, M. Bibes, and A. Zunger, Phys. Rev. B **98**, 075135 (2018).

[18] A. W. Sleight, Phys. C: Supercond. Appl. **514**, 152 (2015).
[19] J. Varignon, M. N. Grisolia, J. Íñiguez, A. Barthélémy, and M. Bibes, npj Quantum Mater. **2**, 21 (2017).
[20] A. Mercy, J. Bieder, J. Íñiguez, and P. Ghosez, Nat. Commun. **8**, 1677 (2017).
[21] J. Varignon, M. Bibes, and A. Zunger, Nat. Commun. **10**, 1658 (2019).
[22] J. Varignon, M. Bibes, and A. Zunger, Phys. Rev. B **100**, 035119 (2019).
[23] J. W. Furness, Y. Zhang, C. Lane, I. G. Buda, B. Barbiellini, R. S. Markiewicz, A. Bansil, and J. Sun, Commun. Phys. **1**, 11 (2018).
[24] C. Lane, J. W. Furness, I. G. Buda, Y. Zhang, R. S. Markiewicz, B. Barbiellini, J. Sun, and A. Bansil, Phys. Rev. B **98**, 125140 (2018).
[25] Y. Hinuma, H. Hayashi, Y. Kumagai, I. Tanaka, and F. Oba, Phys. Rev. B **96**, 094102 (2017).
[26] L. Iglesias, M. Bibes, and J. Varignon, Phys. Rev. B **104**, 035123 (2021).
[27] J. Varignon, npj. Comp. Mater. **9**, 30 (2023).
[28] M. Ekholm, D. Gambino, H. J. M. Jönsson, F. Tasnádi, B. Alling, and I. A. Abrikosov, Phys. Rev. B **98**, 094413 (2018).
[29] Y. Zhang, W. Zhang, and D. J. Singh, Phys. Chem. Chem. Phys. **22**, 19585 (2020).
[30] D. A. Pantazis, Magnetochemistry **5**, 69 (2019).
[31] Y. Fu and D. J. Singh, Phys. Rev. Lett. **121**, 207201 (2018).
[32] E. B. Isaacs and C. Wolverton, Phys. Rev. Mater. **2**, 063801 (2018).
[33] D. Mejía-Rodríguez and S. B. Trickey, Phys. Rev. B **100**, 041113(R) (2019).
[34] Y. Fu and D. J. Singh, Phys. Rev. B **100**, 045126 (2019).
[35] A. J. Garza and G. E. Scuseria, J. Phys. Chem. Lett. **7**, 4165 (2016).
[36] R. Gillen, S. J. Clark, and J. Robertson, Phys. Rev. B **87**, 125116 (2013).
[37] J. L. F. Da Silva, M. V. Ganduglia-Pirovano, J. Sauer, V. Bayer, and G. Kresse, Phys. Rev. B **75**, 045121 (2007).
[38] A. Savin, J. Chem. Phys. **153**, 160901 (2020).
[39] S. Khalid, A. Sharan, and A. Janotti, Phys. Rev. B **101**, 125105 (2020).
[40] P. E. Blöchl, Phys. Rev. B **50**, 17953 (1994).
[41] T. R. McGuire, M. W. Schafer, R. J. Joenk, H. A Alperin, and S. J. Pickart, J. Appl. Phys. **37**, 981 (1966).
[42] J. Khler, R. Dinnebier, and A. Bussmann-Holder, Phase Transitions **85**, 949 (2012).
[43] J. H. Lee, X. Ke, N. J. Podraza, L. F. Kourkoutis, T. Heeg, M. Roeckerath, J. W. Freeland, C. J. Fennie, J. Schubert, D. A. Muller *et al.*, Appl. Phys. Lett. **94**, 212509 (2009).
[44] A. C. Komarek, H. Roth, M. Cwik, W. D. Stein, J. Baier, M. Kriener, F. Bourée, T. Lorenz, and M. Braden, Phys. Rev. B **75**, 224402 (2007).
[45] D. J. Lovinger, E. Zoghlin, P. Kissin, G. Ahn, K. Ahadi, P. Kim, M. Poore, S. Stemmer, S. J. Moon, S. D. Wilson *et al.*, Phys. Rev. B **102**, 085138 (2020).
[46] M. N. Grisolia, F. Y. Bruno, D. Sando, H. J. Zhao, E. Jacquet, X. M. Chen, L. Bellaiche, A. My Barthélé, and M. Bibes, Appl. Phys. Lett. **105**, 172402 (2014).
[47] L. Bjaalie, A. Verma, B. Himmetoglu, A. Janotti, S. Raghavan, V. Protasenko, E. H. Steenbergen, D. Jena, S. Stemmer, and C. G. Van de Walle, Phys. Rev. B **92**, 085111 (2015).
[48] R. Mguedla, A. Ben Jazia Kharrat, M. Saadi, K. Khirouni, N. Chniba-Boudjada, and W. Boujelben, J. Alloys Compd. **812**, 152130 (2020).
[49] S. Lei, L. Liu, C. Wang, C. Wang, D. Guo, S. Zeng, B. Cheng, Y. Xiao, and L. Zhou, J. Mater. Chem. A **1**, 11982 (2013).
[50] N. Shamir, H. Shaked, and S. Shtrikman, Phys. Rev. B **24**, 6642 (1981).
[51] R. Mguedla, A. Ben Jazia Kharrat, O. Taktak, H. Souissi, S. Kammoun, K. Khirouni, and W. Boujelben, Opt. Mater. (Amst). **101**, 109742 (2020).
[52] C. Ritter, R. Vilarinho, J. A. Moreira, M. Mihalik, M. Mihalik, and S. Savvin, J. Phys. Condens. Matter **34**, 265801 (2022).
[53] Y. Tokunaga, S. Iguchi, T. Arima, and Y. Tokura, Phys. Rev. Lett. **101**, 097205 (2008).
[54] M. A. Butler, D. S. Ginley, and M. Eibschutz, J. Appl. Phys. **48**, 3070 (1977).
[55] S. Y. Smolin, M. D. Scafetta, G. W. Guglietta, J. B. Baxter, and S. J. May, Appl. Phys. Lett. **105**, 022103 (2014).
[56] G. Kresse, J. Non. Cryst. Solids **192**, 222 (1995).
[57] G. Kresse and J. Furthmüller, Comput. Mater. Sci. **6**, 15 (1996).
[58] G. Kresse and J. Hafner, Phys. Rev. B **48**, 13115 (1993).
[59] V. Popescu and A. Zunger, Phys. Rev. B **85**, 085201 (2012).
[60] http://staff.ustc.edu.cn/~zqj/
[61] A. M. Glazer, Acta Cryst. B **28**, 3384 (1972).
[62] J. Varignon, M. N. Grisolia, D. Preziosi, P. Ghosez, and M. Bibes, Phys. Rev. B **96**, 235106 (2017).
[63] D. Li, K. Lee, B. Y. Wang, M. Osada, S. Crossley, H. R. Lee, Y. Cui, Y. Hikita, and H. Y. Hwang, Nature (London) **572**, 624 (2019).
[64] M. Osada, B. Y. Wang, B. H. Goodge, K. Lee, H. Yoon, K. Sakuma, D. Li, M. Miura, L. F. Kourkoutis, H. Y. Hwang, M. Osada, and H. Y. Hwang, Nano Lett. **20**, 5735 (2020).
[65] M. Osada, B. Y. Wang, B. H. Goodge, S. P. Harvey, K. Lee, D. Li, L. F. Kourkoutis, and H. Y. Hwang, Adv. Mater. **33**, 2104083 (2021).
[66] Á. A. Carrasco Álvarez, S. Petit, L. Iglesias, W. Prellier, M. Bibes, and J. Varignon, Phys. Rev. Res. **4**, 023064 (2022).
[67] Y. Zhang, J. Zhang, X. He, J. Wang, and P. Ghosez, arXiv:2201.00709.
[68] C. Xia, J. Wu, Y. Chen, and H. Chen, Phys. Rev. B **105**, 115134 (2022).
[69] F. Bernardini, A. Bosin, and A. Cano, Phys. Rev. Mater. **6**, 044807 (2022).